PAPER

Liquid–gas support and lubrication based on a ferrofluid seal

IOP Publishing Journal of Physics D: Applied Physics
J. Phys. D: Appl. Phys. **53** (2020) 025002 (7pp) https://doi.org/10.1088/1361-6463/ab4c0c

Liquid–gas support and lubrication based on a ferrofluid seal

Zhengdong Hu, Qingwen Dai, Wei Huang and Xiaolei Wang

National Key Laboratory of Science and Technology on Helicopter Transmission, Nanjing University of Aeronautics and Astronautics, Yudao Street 29#, Nanjing 210016, People's Republic of China

E-mail: huangwei@nuaa.edu.cn

Received 21 January 2019, revised 19 September 2019
Accepted for publication 8 October 2019
Published 29 October 2019

Abstract

The use of a lubricated bearing is an effective way to reduce friction. In contrast to traditional hydrostatic and hydrodynamic bearings, a type of liquid–gas mixed supporting construction based on a ferrofluid seal was introduced in this paper. When the undersurface of a magnet ring bonds to a plate, ferrofluids absorbed on the upper surface of the magnet can supply bearing capacity generated by the magnetized fluid and the compressible gas sealed in the ring chamber. The supporting forces of the liquid, gas and liquid–gas mix based on a ferrofluid seal were tested. To further increase the supporting capacity, two simple methods were suggested. The low-friction properties of this supporting structure were also confirmed. The advantage of the construction is that the supporting forces are adjustable and independent of any other external facilities or relative movement. Such a design provides the underlying applications for precision and low-velocity mechanisms.

Keywords: ferrofluids, supporting force, magnetic property, seal

(Some figures may appear in colour only in the online journal)

1. Introduction

Friction is a widespread physical phenomenon and it can be ascribed to the interactions between the material zones of bodies that are in contact or moving relative to one another. Furthermore, the interaction of friction between contacting bodies encompasses the scale of global tectonic plates to atomic dimensions [1]. It is hard to imagine the world without friction.

However, in a mechanical system, friction is frequently undesirable. Lubricated bearings are an effective way to reduce friction due to the existence of an oil film between moving bodies. In this respect, hydrostatic [2] and hydrodynamic bearings [3] are two successful examples. For hydrostatic lubrication, a pump outside the bearing produces the oil pressure and the hydrodynamic bearings obtain the load carrying capacity by relative movement. Such restrictions on the formation of the oil film pressure limit the application of the two types of bearings to a certain extent, especially in precision and low-velocity mechanisms. Questions then arise: do other types of lubricated bearings exist which can produce load carrying capacity under low velocity or even in static situations? Can this type of bearing capacity be afforded by liquid and gas together?

To this aim, bearings lubricated with smart ferrofluids (FFs) have been developed [4–7]. FFs are stable colloidal suspensions of nano-sized magnetite particles dispersed in a liquid medium by a suitable surfactant [8, 9]. They manifest common liquid performances combined with magnetic properties. In the presence of a magnetic field, the randomly oriented poles of the magnetic particles in FFs will be aligned along the external field, presenting magnetization characteristics. The inset of figure 1 shows a liquid ring of FFs absorbed on the surface of an annular magnet. Previous studies [10, 11] have shown that the gas in the chamber sealed by the FFs can produce a supporting force when the undersurface of the magnet ring is bonded to a plate. Besides the gas support, the magnetized FFs may also generate liquid support due to the magnetic volumetric force [12]. However, in such an FF sealed structure, the liquid part is often overlooked.

Figure 1 shows a sketch map of such an FF supporting construction, and the total supporting force (F) is shared by the sealed gas (F_G) and magnetized liquid (F_L) together. The advantage of this supporting system is that the bearing ability

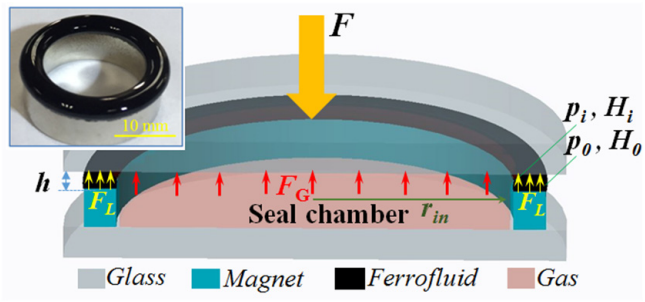

Figure 1. A sketch map of the FF supporting construction. (The inset shows an image of a magnet ring absorbed with FFs.)

is independent of pumps or relative movement, which is quite different from traditional hydrostatic and hydrodynamic bearings. In addition, given the compressibility of the gas and liquid, the total supporting force (F) is adjustable according to the supporting height (h) of the FF film, revealing the adaptive nature of load bearing.

In such supporting systems, studies have mainly focused on the gas support and little attention has been paid to the liquid part. The load carrying capacity was approximately considered coming from the sealed gas and was evaluated by measuring the normal force. However, in the total supporting force (F), what are the particular contributions of the gas (F_G) and liquid (F_L)? Furthermore, what about the specific variation in the pressure in the chamber during the loading process? In addition, with the exception of using the ferromagnetic material around the magnet [13], are there any other methods to enhance the load carrying capacity (F)? In this paper, to verify each contribution, experiments were carried out to measure the chamber pressure, the liquid and the total liquid–gas mixed supports of such an FF bearing. The gas support obtained from the chamber pressure was compared with the theoretical results. Then, to further increase the supporting capacity, two simple methods were suggested: (1) using the FFs with higher magnetization; (2) using two magnet-ring nested structures. Finally, friction tests were carried out to further confirm the superiority of such a support system in the lubrication area.

2. Experimental details

2.1. Magnets and FFs

In this paper, two axial-magnetized NdFeB annular permanent magnets of different sizes (Ring 1: Φ30 mm × Φ25 mm × 5 mm; Ring 2: Φ20 mm × Φ15 mm × 5 mm) are used. The original surface magnetic strength of Ring 1 is 316 mT, and Ring 2 is 270 mT. To achieve adequate surface magnetic strength, parts of the magnet (Ring 1) were heated in a vacuum oven and the value of the processed magnets was approximately 270 mT.

Commercial kerosene-based FFs comprised of Fe_3O_4 magnetite particles were purchased from Hangzhou Jikang New Materials Co., LTD. To prevent aggregation, the Fe_3O_4 particles with an average size of 15 nm were stabilized using oleic acid as a surfactant. The three FF samples had saturation magnetizations (M_s) of 7.9 kA m^{-1}, 23.9 kA m^{-1} and 39.8 kA m^{-1} with different viscosities (30, 60 and 100 cp, 25 °C). The approximate fractions of the particles in each FF were 1.6 vol.%, 4.9 vol.% and 8.3 vol.%.

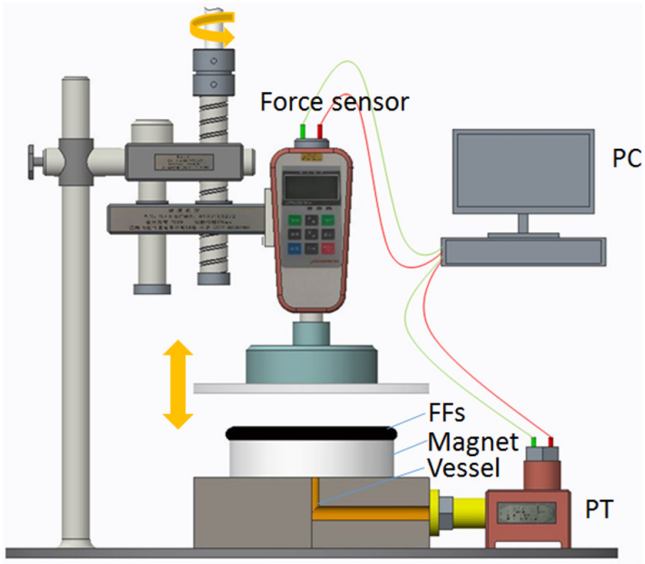

Figure 2. A schematic diagram of the supporting force test platform.

2.2. Supporting force measurement

Figure 2 presents a schematic diagram of the supporting force test platform. The upper glass plate connected with a force sensor was driven in a vertical direction through a screw transmission. The moving speed was fixed at 0.01 mm s^{-1}. The maximum span and resolution of the force sensor were 20 N and 0.01 N, respectively. In addition, to acquire the real-time pressure in the chamber, a pressure transmitter (PT) with a range of 15 kPa was mounted with the sample stage. The sealed chamber of the magnet ring was connected to the PT through a machined vessel inside the stage. As the upper plate contacted with the FF ring, the data from the supporting force and the pressure inside the sealed chamber over the axial displacement of the upper plate were collected by the data acquisition system. To avoid rigid contact, each test was ceased when the height between the upper glass and magnet was 0.01 mm.

Two sets of experiments were carried out: (1) a single magnet ring covered with different FFs; (2) two magnets with concentric nested structures. The inset of figure 1 shows an image of an FF ring formed on a single magnet. Figure 3 presents the nested structures of two magnets with the same surface magnetic strength (270 mT). As shown in figure 3(a), the nested structure with the same magnetic pole arrangement is marked as the N–N type, while the different pole arrangement is marked as the N–S type. Given the different circumferences of the magnets, doses of 0.35 ml and 0.18 ml FFs were dropped for Ring 1 and Ring 2. The appearance of FFs on the two nested structures show significant differences, and the reason for this may be because of the different magnetic field distributions on the magnet ring surfaces (see figure 8).

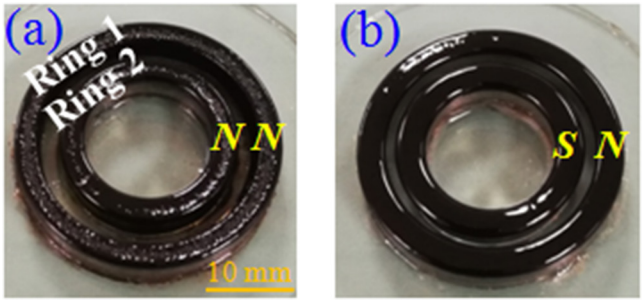

Figure 3. Images of two magnet nested structures absorbed with FFs.

2.3. Frictional force measurement

Lubrication behavior of the bearing system was characterized by measuring the frictional forces using a reciprocation tribotester (Sinto Scientific, JAP). The tester contained an upper stationary holder where a glass plate was fixed and a reciprocating table where the magnet ring absorbed with FFs was placed. The horizontal glass contacted with the FF ring, which shifted with the reciprocating table at an average speed of 0.1 mm s^{-1}. To confirm the bearing effect, the dead load used depended on the supporting test results. The frictional force was recorded by a force transducer throughout the sliding process, and the coefficient of friction was the ratio of the friction force and dead load.

3. Results and discussion

Figure 4 presents the relationship between the supporting force and the height (h). Note that all the forces enhance as the upper plate approaches the magnet's surface. For the magnet ring with the bottom unsealed, the force (F_L) (the black line in figure 4) only comes from the magnetic volumetric force of the magnetized liquid. As mentioned above, each particle in FFs can be considered as a permanent magnet with embedded magnetic moments. In the presence of an applied field, the magnetic moment of the particles will be oriented along the magnetic field, leading to magnetization. The magnetization process of the FFs generates an attractive force in each particle, which presents itself as a magnetic volumetric force or magnetic pressure in the liquid. This force may serve as liquid support during the pressing course. In the general case, the magnetic volumetric force is proportional to the magnetic field strength through magnetization and the magnetic field gradient [14]. When the plate moves down continuously, the magnetic field strength as well as the gradient fastened on the FFs is stronger. Thus, the liquid supporting force (F_L) increases gradually.

For the bottom-sealed condition, the supporting force (the blue line in figure 4) originates from the liquid and the gas together. The mixed supporting force increased obviously with the participation of the gas. In the testing course, the chamber pressure detected by the PT was transformed into the gas supporting force by multiplying the supporting area (the red line in figure 4). As can be seen, the gas support is much higher than that of the liquid part. It can be deduced

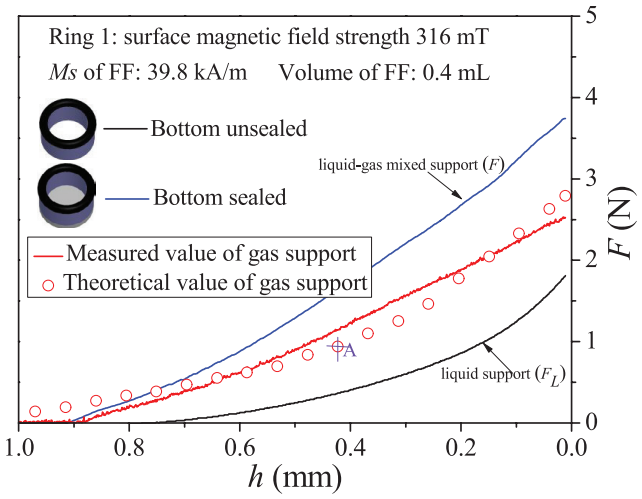

Figure 4. Supporting forces plotted as a function of the height. The lines present the measured data, and the open circles are the theoretical values of the gas supporting force calculated according to equation (2).

that the gas support plays a major contribution in the mixed supporting force.

The theory of gas support in the sealed chamber can be simply explained as follows. As described in figure 1, when neglecting the gravity and surface tension of the FFs, based on the principle of FF sealing, the differential pressure between the inner and outer interfaces of FFs can be determined as [15, 16]:

$$p_i - p_0 = \mu_0 \int_{Ho}^{Hi} M\, dH = \mu_0 M\,(H_i - H_0), \qquad (1)$$

where p_i and p_0 are the hydrostatic pressures at the inner and outer boundaries of the FFs, and H_i and H_0 are the respective magnetic field strengths imposed on the fluid interfaces. Here, μ_0 is the permeability of vacuum, M is the magnetization of FFs and its value is a function of the external magnetic field. Because the magnetic field strength in the sealing gap is up to 10^5 A m^{-1}, the FF is in the saturation state (M_s). Therefore, the pressure in the sealed chamber depends on the magnetic field strength of the fluid–air interface. And the gas supporting force (F_G) can be achieved by integrating the pressure over the bearing area($A_F = \pi\ r_{in}^2$, see figure 1):

$$F_G = \int_S (p_i - p_0) \cdot dA_F = \mu_0 M_s\,(H_i - H_0)\,\pi\ r_{in}^2\,. \qquad (2)$$

It can be found that the force (F_G) is mainly determined by the FF sealing capacity according to equation (2). The value is merely affected by the magnetic characteristics of the magnet ring and the FFs. As shown in figure 1, pressing the upper plate not only alters the fluid outline but changes the corresponding magnetic field strength. The inner surface of the FF shifts to the higher magnetic strength, while the outer moves to the lower because of extrusion and radial displacement. Therefore, the force (F_G) enhances with the decreasing height (h) of the upper plate.

To verify the measurement, theoretical calculation of the gas supporting force was performed according to equation (2),

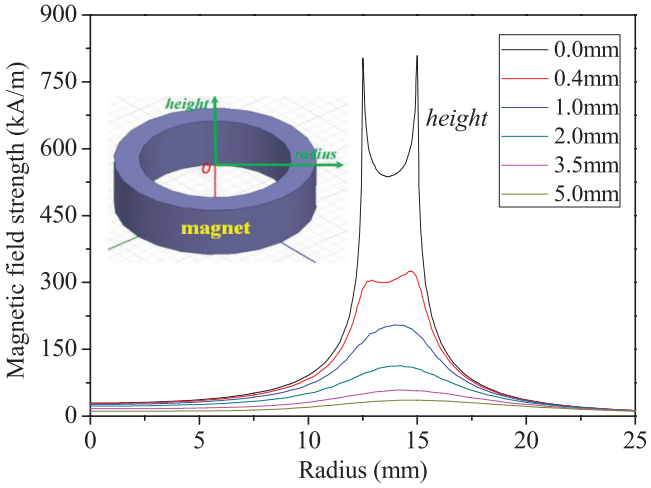

Figure 5. The distribution of the magnetic field at different heights along the magnet radius.

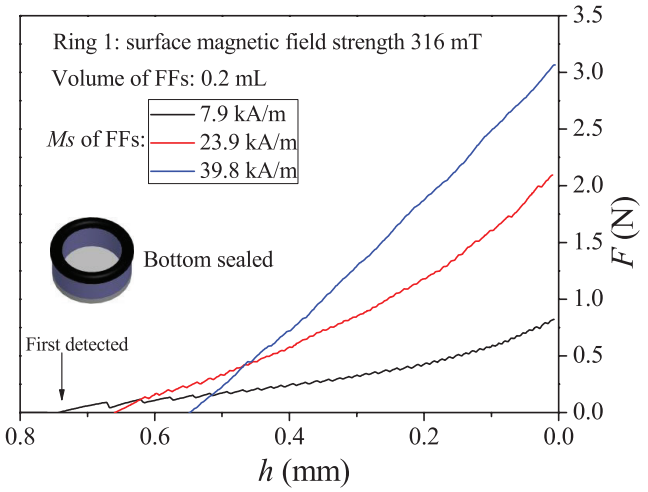

Figure 6. The effect of magnetization of FFs on the mixed supporting forces.

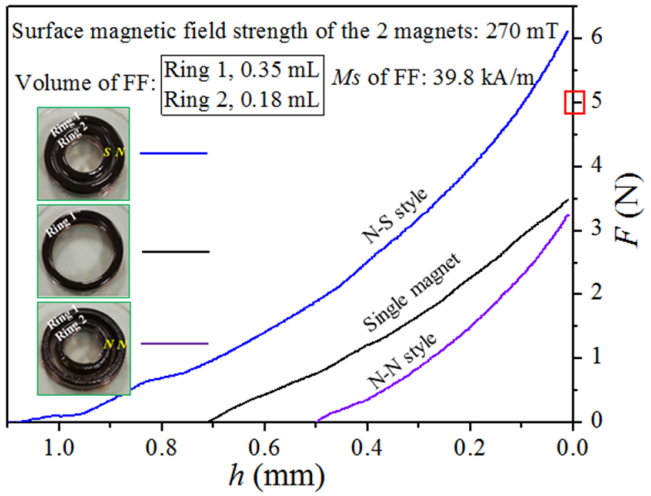

Figure 7. The effect of nested structures on the mixed supporting forces. (All samples are bottom sealed.)

and the computational model is described in figure 1. As the upper plate shifts down, the bearing capacity of the sealed chamber relies on the magnetic field strength of the fluid–air interfaces. To achieve the field distribution of the magnet ring, the magnetic field finite element method (FEM) was used, neglecting the effect of FFs. The parameters of the dimensional and magnetic imported were in agreement with the magnet ring sample (Φ30 mm × Φ25 mm × 5 mm, remanence B_r: 1.18 T, coercivity H_c: −880 kA m^{-1} and relative permeability μ_r: 1.1). Detailed magnetic field computation can be found in [17]. Figure 5 shows the distributions of the magnetic field above the magnet ring at different heights along the radius direction. For a fixed supporting height, considering the incompressibility, the location of the fluid–air boundary may be determined approximately by the volume of the FFs. Thus, the corresponding values of the magnetic fields at the fluid interfaces can be achieved, and the final theoretical gas support can also be calculated. For example, when the volume of the FF is 0.4 ml and the height (h) is 0.42 mm, the magnetic field strengths (H_i and H_0) at the fluid locations are 2.99 × 10^5 A m^{-1} and 2.61 × 10^5 A m^{-1}, respectively. The permeability of vacuum (μ_0) is 4π × 10^{-7} N A^{-2}, and the supporting area ($A_F = \pi\, r_{in}^2$) is 4.91 × 10^{-4} m^2. The magnetization (M_s) of the FFs is 3.98 × 10^4 A m^{-1}. The calculated value is about 0.93 N (point A in figure 4), which is close to the measured value. As shown in figure 4 (red circle), the calculated forces exhibit similar tendencies to the measured gas supporting force in general.

Figure 6 presents the effect of magnetization (M_s) of FFs on the liquid–gas mixed supporting forces. As can be seen, the forces are enhanced with the increase in M_s. As is known, the M_s of FFs is related to the concentration of the magnetic particles dispersed in the carrier liquid. On one side, with the increase in M_s, the attractive force between particle per unit volume increases, which will boost the magnetic volumetric force of the fluid (F_L). Given the effect of viscosity, the liquid support part may also be enhanced due to the increased viscosity resistance of the FFs. On the other side, the gas supporting force (F_G) will grow with the M_s according to equation (2).

Besides the forces, note that the curve using FFs with an M_s of 39.8 kA m^{-1} is close to a straight line, which means the support stiffness of the bearing system also increases with the increasing M_s. One more thing that should be explained is that the height of the FF covering on the magnet decreases with the increase in M_s due to the enhanced absorption. This is the reason why the detected force first appears when using the FFs with the lowest M_s of 7.9 kA m^{-1}.

To further enhance the bearing capacity per unit area, attempts have been made to design the nested structures of two annular magnets. Figure 7 presents the effect of the magnetic pole arrangement of the nested structure on the mixed supporting force. For comparison, the force of a single magnet (Ring 1) with the same surface magnetic field strength (270 mT) was also measured. Although the same magnets were used, the forces supplied by the two nested structures were quite different. The bearing capacity of the sample with

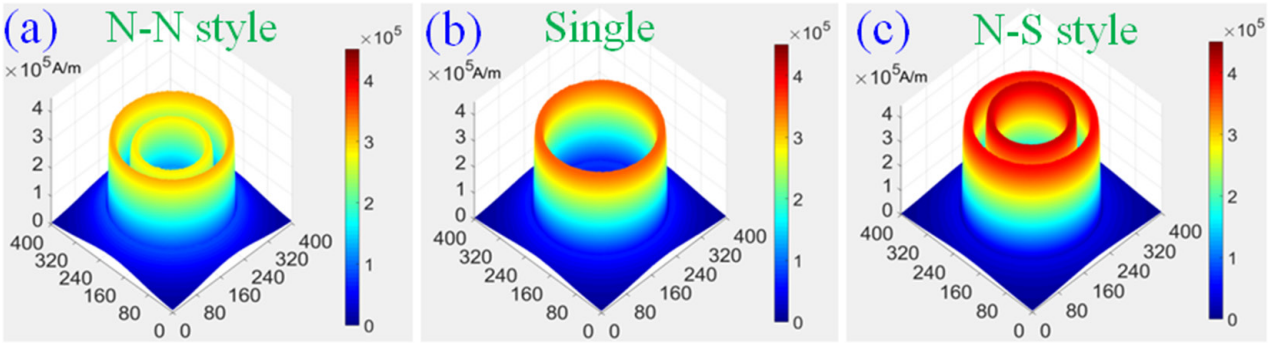

Figure 8. A 3D-visualization of the surface magnetic field for the nested structures and single magnet.

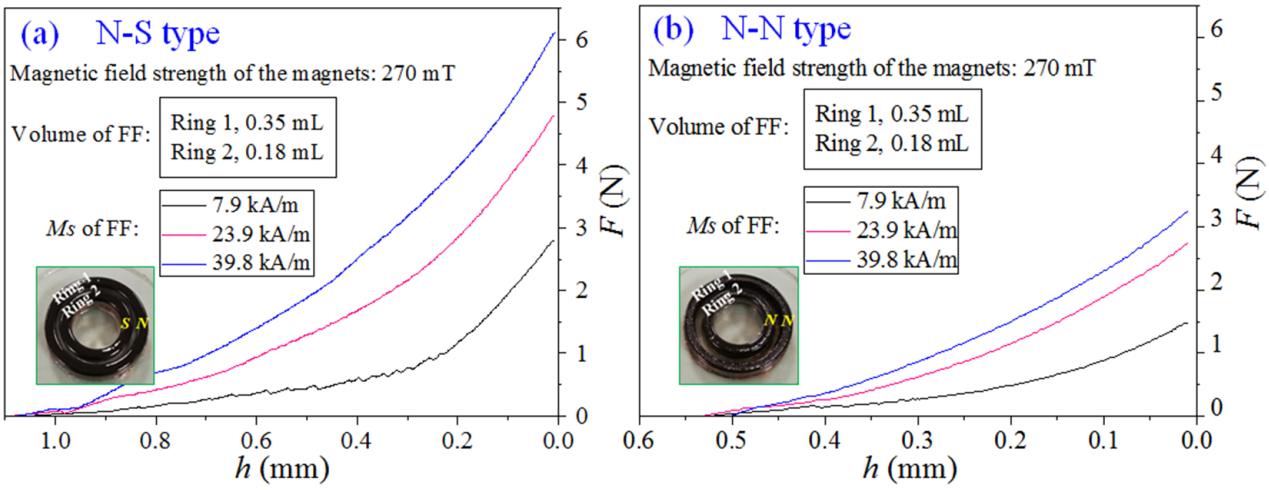

Figure 9. The effect of the magnetization of FFs on the supporting forces for the nested structures.

the N–S type (6.1 N) rises dramatically compared with the N–N type (3.2 N), and the growth of the maximum force hits 90.6%. More interestingly, the bearing capacity of the N–N type is even lower than that of the single magnet ring (3.5 N).

To understand the above phenomena, the surface magnetic field distributions of the three samples were analyzed using an Ansoft Maxwell 3D model. Figure 8 gives the calculated results of the 3D-visualization of the surface magnetic field strength. For the N–N type sample, in view of the magnetic law, like poles repel and the magnetic flux lines on the two adjacent interfaces are mutually exclusive. The magnets will turn to the status of the lower magnetic energy, and thus the surface magnetic field strength on each magnet is generally lower than that of the single magnet (see figures 8(a) and (b)). In figure 8(c), a significant increment of surface magnetic field is observed for the N–S type sample. The magnetic flux line is always along the direction with the smallest magnetic reluctance. Based on the 'unlike poles attract' rule, a magnetic flux line circuit will be formed between the neighboring magnet interfaces, and the surface magnetic flux density on each magnet surface will enhance markedly. Thus, the magnets arranged in the N–S style express a higher surface magnetic field strength.

As mentioned above, the bearing capacity of the nested structures is also related to the magnetic field. The increased magnetic field will improve the attractive force on each particle. Therefore, the liquid supporting force is enhanced. Moreover, the gas supporting part is also increased with the increasing magnetic field according to equation (2). Combining these two aspects, the mixed supporting force of the N–S type is higher than that of the N–N type.

Meanwhile, the N–S type sample also demonstrates a higher supporting performance than that of the single magnet. Referenced by the principle of the FF multistage seal [18], each magnet in the nested structures may be considered as one sealing stage. Compared with the single stage FF seal (the single magnet), two stages can be used to build up the pressure differential in each stage and to maintain the larger differential pressures. Moreover, due to the existence of Ring 2, the decreased volume of the seal chamber may also lead to a quick increment of the pressure based on the ideal gas equation. Through a combination of these factors, the nested structure of the N–S type presents a better bearing performance.

Figure 9 shows the effect of the magnetization of FFs on the supporting forces for the two nested structures. The experimental data further verify two results drawn above. The first is that the higher supporting forces can be obtained by using the FFs with higher magnetization. The second is that the nested structure of the N–S type can supply a larger bearing capacity compared with the N–N type. Both of these methods are simple and effective.

In this work, the purpose of support is to achieve full fluid lubrication. Figure 10 presents the friction curves of the nested structures at a low sliding speed. The two magnetic samples

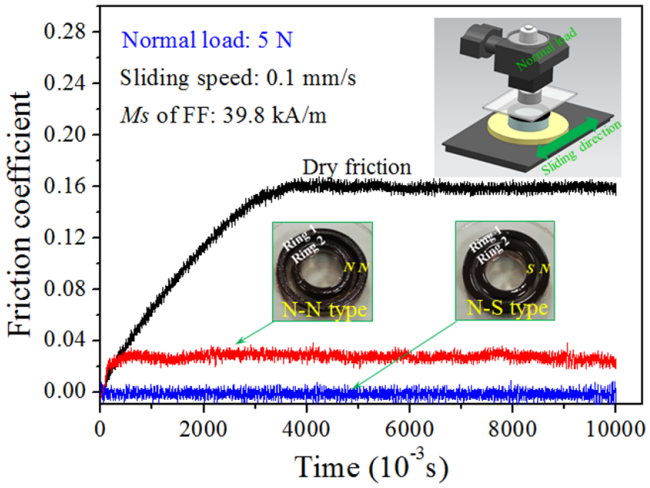

Figure 10. Friction curves of the nested structures. (The magnetic samples and the FF used are the same as that in figure 7.)

and the FFs used are the same as that in figure 7. During the friction process a normal load of 5 N was chosen, and the value was between the maximum bearing capacity of the N–N type (3.2 N) and the N–S type (6.1 N) (see figure 7).

As shown in figure 10, the sample under dry friction conditions showed the highest friction coefficient. And the coefficients declined obviously when lubricated by FFs. For the N–N type sample, the normal load exceeded its supporting force limit (3.2 N, see figure 7). It implies that normal load is carried partly by the supporting force and partly by the asperity contacts. A friction coefficient of 0.03 was obtained and the friction pairs were not separated completely, in which the states of fluid friction and boundary friction coexist.

A fundamental shift in lubrication occurs for the N–S type sample. Since its limit bearing capacity is larger than the normal load, the friction surfaces were totally separated by the magnetized FFs and the sealed gas, like a hydrostatic bearing. And the non-contact state between the friction pairs can also be confirmed by the supporting tests. As shown in figure 7, at the normal load of 5 N, the height between the upper glass and the magnets is about 0.1 mm. Therefore, the friction force only originates from the viscous resistance of the FFs, and the friction coefficient falls close to zero.

For such a construction, the supported element may float when its weight is less than the mixed supporting force, and thus low friction can be achieved. For a tribological system, this type of supporting force is quite important since it does not rely on relative movement or a pump. Compared with traditional hydrodynamic and hydrostatic lubrication, such a design provides a new mode of bearing capacity, which could be applied to precision and low-velocity mechanisms.

4. Conclusions

In summary, we have presented an experimental study of liquid–gas support and lubrication based on an FF seal. The measured force curves show that compared with the liquid supporting part, the gas supporting force is the major contributor of the mixed support. Meanwhile, the theoretical curve of the gas support in terms of the FF sealing theory conforms well to the experimental results. In addition, attempts have been made to further increase the load carrying capacity of the supporting construction. As expected, using FFs with higher saturation magnetization is one of the effective methods, while for the magnet nested structures, the arrangement of the magnetic pole presents a decisive factor. The higher bearing capacity was observed only for the nested structure of the N–S type. Moreover, ultralow friction coefficients could be obtained when the bearing capacity was higher than the normal load.

In view of these results, it seems that liquid and gas supports can be achieved at the same time based on the FF seal construction. Provided the mixed force is larger than the weight of the supporting body, direct contact may be avoided due to the ‘buoyancy’. Such a result is highly desirable for moving components of a mechanical system, and it provides an opportunity for the design of non-contact motions.

Acknowledgments

The authors thank the National Natural Science Foundation of China (No. 51875278) for financial support.

ORCID iDs

Qingwen Dai https://orcid.org/0000-0001-7422-4259
Wei Huang https://orcid.org/0000-0002-8871-634X
Xiaolei Wang https://orcid.org/0000-0002-9055-1011

References

[1] Kligerman Y and Varenberg M 2013 Elimination of stick-slip motion in sliding of split or rough surface *Tribol. Lett.* **53** 395–9
[2] Kang Y, Chen C-H, Lee H-H, Hung Y-H and Hsiao S-T 2011 Design for static stiffness of hydrostatic bearings: single-action variable compensations *Ind. Lubr. Tribol.* **63** 103–18
[3] Andablo-Reyes E, Vicente J, Hidalgo-Álvarez R, Myant C, Reddyhoff T and Spikes H A 2010 Soft elasto-hydrodynamic lubrication *Tribol. Lett.* **39** 109–14
[4] Shi X and Wang Y 2013 Thermal elastohydrodynamic lubrication property contrast studies of different carrier fluid ferrofluid *Chin. J. Mech. Eng.* **49** 106–10
[5] Patel N S, Vakharia D P, Deheri G M and Patel H C 2017 Experimental performance analysis of ferrofluid based hydrodynamic journal bearing with different combination of materials *Wear* **376–7** 1877–84
[6] Shen C, Huang W, Ma G and Wang X 2009 A novel surface texture for magnetic fluid lubrication *Surf. Coat. Technol.* **204** 433–9
[7] Shi X and Wang Y 2012 Elastohydrodynamic lubrication analysis of ferrofluid lubricated lathe spindle bearing *Lubr. Eng.* **37** 41–4
[8] Odenbach S 2003 Ferrofluids—magnetically controlled suspensions *Colloids Surf.* A **217** 171–8
[9] Andablo-Reyes E, Hidalgo-Álvarez R and de Vicente J 2011 Controlling friction using magnetic nanofluids *Soft Matter* **7** 880–3

[10] Lampaert S G E, Spronck J W and van Ostayen R A J 2017 Load and stiffness of a planar ferrofluid pocket bearing *Proc. Inst. Mech. Eng.* J **232** 14–25
[11] Wang Z, Hu Z, Huang W and Wang X 2017 Elastic support of magnetic fluids bearing *J. Phys. D: Appl. Phys.* **50** 435004
[12] Osman T A, Nada G S and Safar Z S 2001 Static and dynamic characteristics of magnetized journal bearings lubricated with ferrofluid *Tribol. Int.* **34** 369–80
[13] Boots A S T, Krijgsman L E, de Ruiter B J M, Lampaert S G E and Spronck J W 2019 Increasing the load capacity of planar ferrofluid bearings by the addition of ferromagnetic material *Tribol. Int.* **129** 46–54
[14] Oldenburg C M, Borglin S E and Moridis G J 2000 Numerical simulation of ferrofluid flow for subsurface environmental engineering applications *Trans. Porous Media* **38** 319–44
[15] Berkovsky B M, Medvedev V F and Krakov M S 1993 *Magnetic Fluids Engineering Applications* (Oxford: Oxford University Press)
[16] Odenbach S 1993 Magnetic fluids *Adv. Colloid Interface Sci.* **46** 263–82
[17] Shahrivar K and de Vicente J 2014 Ferrofluid lubrication of compliant polymeric contacts: effect of non-homogeneous magnetic fields *Tribol Lett.* **56** 281–92
[18] Popplewell J and Charles S W 1981 Ferromagnetic liquids-their magnetic properties and applications *IEEE Trans. Magn.* **17** 2923–8